PAPER

Check for updates

Diffusiophoresis in porous media saturated with a mixture of electrolytes

Siddharth Sambamoorthy [a] and Henry C. W. Chu [*b]

Current theories of diffusiophoresis in porous media are limited to a porous medium saturated with a valence symmetric electrolyte. A predictive model for diffusiophoresis in porous media saturated with a valence asymmetric electrolyte, or a general mixture of valence symmetric and asymmetric electrolytes, is lacking. To close this knowledge gap, in this work we develop a mathematical model, based upon the regular perturbation method and numerical integration, to compute the diffusiophoretic mobility of a colloid in porous media saturated with a general mixture of electrolytes. We model the electrokinetics using the Poisson–Nernst–Planck equations and the fluid transport in porous media using the Brinkman equation with an electric body force. We report three novel key findings. First, we demonstrate that, in the same electrolyte concentration gradient, lowering the permeability of the porous medium can significantly weaken the colloid diffusiophoretic motion. Second, we show that, surprisingly, by using a valence asymmetric electrolyte the colloid diffusiophoretic motion in a denser porous medium can be stronger than that in a less dense porous medium saturated with a symmetric electrolyte. Third, we demonstrate that varying the composition of an electrolyte mixture does not only change the strength of the colloid diffusiophoretic motion drastically, but also qualitatively its direction. The model developed from this work can be used to understand and predict natural phenomena such as intracellular transport, as well as design technological applications such as enhanced oil recovery, nanoparticle drug delivery, and colloidal species separation.

1 Introduction

Diffusiophoresis is the deterministic motion of a colloid induced by a surrounding solute concentration gradient.[1–7] Diffusiophoresis in an ionic solute concentration gradient comprises the chemiphoretic and electrophoretic transport: the chemiphoretic transport is driven by an osmotic pressure gradient and the electrophoretic transport is driven by an electric field; both the osmotic pressure gradient and the electric field are induced by the solute concentration gradient. Diffusiophoresis is pivotal in natural settings such as intracellular transport[8–11] and is increasingly utilized in applications such as enhanced oil recovery,[12–15] nanoparticle drug delivery,[16,17] and colloidal species separation.[18–41] The diffusiophoretic velocity follows $\boldsymbol{u} = M\nabla \log n$, where n is the ion number density and M is the diffusiophoretic mobility. A positive (negative) M corresponds to a colloid driven up or down the solute concentration gradient. The mobility is the key to quantify diffusiophoresis and encompasses physical properties of the colloid and the surrounding media. The objective of this

article is to develop a predictive model of diffusiophoresis that accounts for the surrounding porous media and a mixture of valence symmetric and asymmetric electrolytes, thereby uncovering and predicting their impacts on diffusiophoresis.

Current theories of diffusiophoresis in a valence asymmetric electrolyte and a mixture of valence symmetric and asymmetric electrolytes have ignored the presence of porous media. Pawar *et al.*[42] developed the first theory of diffusiophoresis in a valence asymmetric electrolyte, where the colloid electric double layer thickness κ^{-1} is infinitesimally thin relative to the colloid radius a, *i.e.*, $\kappa a \gg 1$. Bhattacharyya *et al.*[43,44] derived a general model that accounts for arbitrary values of the colloid surface potential ζ and κa. Wilson *et al.*[45] measured the colloid diffusiophoretic mobility in a valence asymmetric electrolyte in experiments and obtained good agreement with prior theories. Chiang and Velegol[46] developed the first theory of diffusiophoresis in a mixture of electrolytes. Their theory assumes that $\kappa a \gg 1$ and ζ is low compared to the thermal voltage kT/e, where k is the Boltzmann constant, T is the absolute temperature, and e is the proton charge. Shi *et al.*[19] derived a more general expression for the diffusiophoretic mobility, by relaxing the assumption of $\zeta \ll kT/e$. Gupta *et al.*[47] and Ohshima[48] presented approximate expressions for the mobility in the limit of $\zeta \ll 1$, $\zeta \gg 1$, and $\kappa a \gtrsim 50$. Samanta *et al.*[49] derived a general model that accounts for $\kappa a \gtrsim 50$ and arbitrary values of ζ.

aDepartment of Chemical Engineering, University of Florida, Gainesville, FL 32611, USA

bDepartment of Chemical Engineering and Department of Mechanical and Aerospace Engineering, University of Florida, Gainesville, FL 32611, USA. E-mail: h.chu@ufl.edu

Current theories of diffusiophoresis in porous media are not applicable to a valence asymmetric electrolyte nor a mixture of electrolytes, and are limited to a valence symmetric electrolyte, *i.e.*, two ionic species with valence $z_1 = -z_2 = z$. Recently, our group pioneered a theory for diffusiophoresis in porous media.[50] The theory models the hydrodynamic interactions between the colloid and the porous media, which act to dampen the colloid motion as the porous medium permeability decreases. The model accurately captures diffusiophoresis experiments by Doan *et al.*[17] with no adjustable parameters, where collagen gels are used as the porous media. Bhaskar and Bhattacharyya[51] incorporated the effect of ion size into the theory, showing quantitatively different predictions. Somasundar *et al.*[52] demonstrated the feasibility of diffusiophoresis in another porous medium, by driving colloids through porous bacterial films using a concentration gradient of a valence symmetric electrolyte. Jotkar *et al.*[53,54] and Alipour *et al.*[55] conducted pore-scale simulations and microfluidic experiments to examine the effect of diffusiophoresis on the hydrodynamic dispersion in porous media with different degrees of water saturation and geometric disorder. However, currently it is lacking a model that can simulate diffusiophoresis in porous media saturated with a valence asymmetric electrolyte or a general mixture of valence symmetric and asymmetric electrolytes.

In this work, we develop a mathematical model to predict the colloid diffusiophoretic mobility in a porous medium saturated with a general mixture of valence symmetric and asymmetric electrolytes. We employ the Poisson–Nernst–Planck equations to model the ion transport and electric potential distribution, and the Brinkman equation with an electric body force to model the fluid transport in a porous medium. We solve the equations using a combination of the regular perturbation method and numerical integration. We report three novel key findings that highlight the coupled effects of porous media and electrolyte mixtures on diffusiophoresis. First, we show that in the same electrolyte concentration gradient the colloid diffusiophoretic motion is significantly weaker in a less permeable porous medium. This is consistent with the fundamental nature of porous media in dampening hydrodynamics,[56,57] and generalizes the same conclusion that was made in prior work for a valence symmetric electrolyte[17,50–55] to a valence asymmetric electrolyte and a general mixture of electrolytes. Second, we show that by using a valence asymmetric electrolyte, surprisingly, diffusiophoresis in a denser porous medium can be stronger than that in a less dense porous medium filled with a valence symmetric electrolyte. This demonstrates the competition between electrokinetics and hydrodynamics, and offers new insights to generate strong diffusiophoresis in porous media using a valence asymmetric electrolyte. Third, we show that, in a mixture of electrolytes, not just the magnitude of the colloid diffusiophoretic motion but qualitatively its direction can change by varying the mixture composition. This highlights the novelty of the present work to leverage valence asymmetric electrolyte and electrolyte mixtures to generate a richer set of diffusiophoresis responses.

The rest of this article is structured as follows. In Section 2, we present the problem formulation for the electrokinetic equations and the diffusiophoretic mobility. In Section 3, we present the results and discussion that elucidate the above-mentioned three key findings. In Section 4, we conclude this study.

2 Problem formulation

Consider a non-conducting colloid of radius a and a constant surface charge density q (or a constant surface potential ζ) in a static porous medium with a constant permeability l^2 and screening length l, subject to a constant concentration gradient of an electrolyte mixture ∇n_i^∞ with $i = 1, 2, …, N$ (Fig. 1). By symmetry, the colloid translates with a constant diffusiophoretic velocity U parallel to ∇n_i^∞ along the z-direction, where U is to be determined. A reference frame moving with U is adopted.

At steady state, ionic species conservation requires that[58]

$$\nabla \cdot j_i = 0 \text{ with } j_i = -D_i \nabla n_i - \frac{D_i z_i e}{kT} n_i \nabla \phi + n_i u, \qquad (1)$$

where j_i, D_i, n_i, and z_i are the flux density, diffusivity, number density, and valence of the i-species, respectively; ϕ is the electric potential, and u is velocity of the electrolyte mixture. The electric potential follows the Poisson equation[58]

$$-\varepsilon \nabla^2 \phi = \rho = \sum_{i=1}^{N} z_i e n_i, \qquad (2)$$

where ε and ρ are the permittivity and space charge density of the electrolyte mixture, respectively. The fluid dynamics in the porous medium is governed by the continuity equation and the Brinkman equation with an electric body force[50,51,59–62]

$$\nabla \cdot u = 0 \quad \text{and} \quad 0 = -\nabla p + \eta \nabla^2 u - \rho \nabla \phi - \eta l^{-2}(u + U), \qquad (3)$$

where p is the pressure and η is the dynamic viscosity of the electrolyte mixture. Modeling the presence of porous media in diffusiophoresis using the Brinkman equation differentiates the present model from the majority of prior work which modeled diffusiophoresis in a free electrolyte solution (in the absence of porous media) using the Stokes equation. The
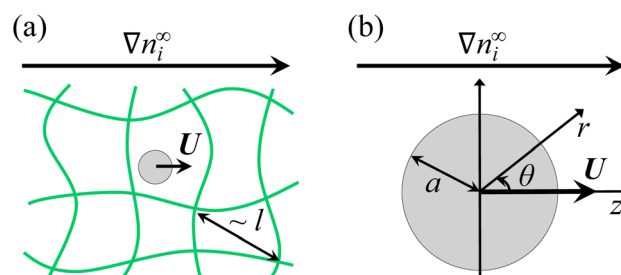

Fig. 1 A concentration gradient of a mixture of N ionic species, ∇n_i^∞ with $i = 1, 2, …, N$, induces the diffusiophoretic motion of a colloid of radius a in a static porous medium with a constant screening length l. The colloid diffusiophoretic velocity U is parallel to ∇n_i^∞. (a) A wholistic view of the colloid and the porous medium. (b) The adopted spherical coordinate and moving reference frame.

Brinkman equation recovers the Stokes equation in a continuous manner as the screening length l approaches infinity. For example, the term $-\eta l^{-2}(\boldsymbol{u} + \boldsymbol{U})$ accounts for the frictional force exerted by the porous medium on the fluid. As $l \to \infty$, this frictional force vanishes, and the Brinkman equation recovers the Stokes equation.

Eqn (1)–(3) are specified by the following boundary conditions. At the colloid surface at $r = a$, no slip and no penetration of the solvent prescribe $\boldsymbol{u} = \boldsymbol{0}$. No penetration of the ionic species prescribes $\boldsymbol{n} \cdot \boldsymbol{j}_i = 0$, where $\boldsymbol{n}$ is the unit normal vector pointing away from the colloid surface. The colloid surface charge density q or surface potential ζ could be specified as $-\boldsymbol{n} \cdot \varepsilon \nabla \phi = q$ or $\phi = \zeta$. Far from the colloid at $r \to \infty$, $\boldsymbol{u} \to -\boldsymbol{U}$ and $p \to p^\infty$, where p^∞ is a reference constant pressure. The ion number densities and their imposed gradients are represented by $n_i \to n_i^\infty + \nabla n_i^\infty \cdot \boldsymbol{r}$, where n_i^∞ is the constant bulk electrolyte concentration and the position vector $\boldsymbol{r}$ is anchored at the centroid of the colloid. To main bulk electroneutrality, the electrolyte concentration gradient induces an electric field $\boldsymbol{E} = -\nabla \phi = (kT/e)\beta \boldsymbol{G}$,[1–3] where $\boldsymbol{G} = (\nabla n_1^\infty)/n_1^\infty = \ldots = (\nabla n_N^\infty)/n_N^\infty$ and $\beta = (\sum_{i=1}^N z_i n_i^\infty D_i)/(\sum_{i=1}^N z_i^2 n_i^\infty D_i)$. The ion diffusivity ratio β controls the magnitude of $\boldsymbol{E}$ and thus the electrophoretic contribution in diffusiophoresis.

In typical diffusiophoresis,[1–3,5,6] the electrolyte concentration gradient at the size of the colloid is much smaller than the background concentration, $\alpha = |\boldsymbol{G}|a \ll 1$. Using the regular perturbation method, we expand the dependent variables in α as

$$n_i = n^\infty \left(\hat{n}_i^0 + \alpha \hat{n}_i^1 \right), \quad \phi = \frac{kT}{e} \left(\hat{\phi}^0 + \alpha \hat{\phi}^1 \right),$$

$$u = \frac{\varepsilon k^2 T^2}{e^2 \eta a} \left(\hat{u}^0 + \alpha \hat{u}^1 \right), \quad p = \frac{\varepsilon k^2 T^2}{e^2 a^2} \left(\hat{p}^0 + \alpha \hat{p}^1 \right), \quad (4)$$

where $n^\infty = 2I = \sum_{i=1}^N z_i^2 n_i^\infty$ is twice the ionic strength of the mixture, and quantities with a superscript 0 (and 1) are associated with the equilibrium (and nonequilibrium) state, where an electrolyte concentration gradient and diffusiophoresis are absent (and present). Quantities with carets are dimensionless. We non-dimensionalize lengths by the colloid radius a and the surface charge density by $\varepsilon kT/(ea)$. Substituting eqn (4) into the governing equations and boundary conditions yield a set of differential equations at different orders of α. Below we present the $O(1)$ perturbation equations and the $O(\alpha)$ perturbation equations for computing the diffusiophoretic velocity and mobility.

2.1 $O(1)$ perturbation equations

The $O(1)$ equations pertains to the equilibrium state where there is no electrolyte concentration gradient and fluid flow, $\boldsymbol{u}^0 = \boldsymbol{0}$. The ionic species conservation and Poisson equation are

$$\widehat{\nabla} \cdot \left(\widehat{\nabla} \hat{n}_i^0 + z_i \hat{n}_i^0 \widehat{\nabla} \hat{\phi}^0 \right) = 0, \quad (5)$$

$$\widehat{\nabla}^2 \hat{\phi}^0 = -\hat{\kappa}^2 \sum_{i=1}^N z_i \hat{n}_i^0, \quad (6)$$

where $\hat{\kappa} = \kappa a$ with $\kappa^{-1} = (\varepsilon kT/e^2 n^\infty)^{1/2}$ being the Debye length. The boundary condition at the colloid surface at $\hat{r} = 1$ is $-n \cdot \nabla \hat{\phi}^0 = \hat{q}$ or $\hat{\phi}^0 = \hat{\zeta}$. The far-field boundary condition at $\hat{r} \to \infty$ are $\hat{n}_i^0 \to \hat{n}_i^\infty$ and $\hat{\phi}^0 \to 0$. Integrating eqn (5) with the boundary condition at $\hat{r} \to \infty$ gives the Boltzmann distribution of the ionic species $\hat{n}_i^0 = \hat{n}_i^\infty \exp(-z_i \hat{\phi}^0)$. Substituting this result into eqn (6) gives the Poisson–Boltzmann equation[58]

$$\frac{1}{\hat{r}^2} \frac{d}{d\hat{r}} \left(\hat{r}^2 \frac{d\hat{\phi}^0}{d\hat{r}} \right) = -\hat{\kappa}^2 \sum_{i=1}^N z_i \hat{n}_i^\infty \exp \left(-z_i \hat{\phi}^0 \right). \quad (7)$$

To solve eqn (7) in a finite computational domain, we consider a sphere of radius $\hat{R}$ that is concentric to and encloses the colloid.[50,63–65] At a sufficiently large $\hat{R} = 1 + 20/\hat{\kappa}$ as in this work, the electric potential decays to zero asymptotically as $(1/\hat{r})\exp(-\hat{\kappa}\hat{r})$. The far-field boundary conditions that were at $\hat{r} \to \infty$ are transformed to $d\hat{\phi}^0/d\hat{r} + (\hat{\kappa} + 1/\hat{R})\hat{\phi}^0 = 0$ at $\hat{r} = \hat{R}$. Eqn (7) is solved using the standard shooting method with the boundary condition at $\hat{r} = 1$ and the transformed far-field boundary condition.

2.2 $O(\alpha)$ perturbation equations

The $O(\alpha)$ equations pertains to the nonequilibrium state. We convert the $O(\alpha)$ equations to a set of ordinary differential equations by introducing the $\hat{\psi}_i^1$ potential, $\hat{n}_i^1 = -z_i \hat{n}_i^0 (\hat{\psi}_i^1 + \hat{\phi}^1)$,[50,63,64] and writing the dependent variables as $\hat{u}_{\hat{r}}^1(\hat{r}, \theta) = -(2/\hat{r})\hat{h} \cos \theta$, $\hat{u}_\theta^1(\hat{r}, \theta) = (1/\hat{r})[d(\hat{r}\hat{h})/d\hat{r}]\sin \theta$, and $\hat{\psi}_i^1(\hat{r}, \theta) = \hat{\psi}_i^1 \cos \theta$, where $\hat{u}_{\hat{r}}^1$ and $\hat{u}_\theta^1$ are the radial and angular components of $\hat{\boldsymbol{u}}^1$, respectively. The $O(\alpha)$ equations now reduce to solving for $\hat{h} = \hat{h}(\hat{r})$ and $\hat{\psi}_i^1 = \hat{\psi}_i^1(\hat{r})$, which are governed by

$$\frac{d^2\hat{\psi}_i^1}{d\hat{r}^2} + \frac{2}{\hat{r}} \frac{d\hat{\psi}_i^1}{d\hat{r}} - \frac{2}{\hat{r}^2}\hat{\psi}_i^1 - z_i \frac{d\hat{\phi}^0}{d\hat{r}} \frac{d\hat{\psi}_i^1}{d\hat{r}} + 2Pe_i \frac{d\hat{\phi}^0}{d\hat{r}} \frac{\hat{h}}{\hat{r}} = 0, \quad (8)$$

$$\frac{d^4\hat{h}}{d\hat{r}^4} + \frac{4}{\hat{r}} \frac{d^3\hat{h}}{d\hat{r}^3} - \frac{4}{\hat{r}^2} \frac{d^2\hat{h}}{d\hat{r}^2} - \gamma^2 \left(-\frac{2}{\hat{r}^2}\hat{h} + \frac{2}{\hat{r}} \frac{d\hat{h}}{d\hat{r}} + \frac{d^2\hat{h}}{d\hat{r}^2} \right)$$
$$+ \frac{\hat{\kappa}^2}{\hat{r}} \frac{d\hat{\phi}^0}{d\hat{r}} \sum_{i=1}^N z_i^2 \hat{n}_i^0 \hat{\psi}_i^1 = 0, \quad (9)$$

where $\gamma = a/l$ and the Peclet number $Pe_i \equiv \varepsilon k^2 T^2/(\eta e^2 D_i)$ describes the ratio of the advective to diffusive transport of the i-species. The boundary conditions at the colloid surface at $\hat{r} = 1$ are $d\hat{\psi}_i^1/d\hat{r} = 0$, $\hat{h} = 0$, and $d\hat{h}/d\hat{r} = 0$. The far-field boundary conditions at $\hat{r} \to \infty$ are $\hat{\psi}_i^1 \to (\beta - 1/z_i)\hat{r}$ and $\hat{h} \to \hat{M}\hat{r}/2$. The non-dimensionalized diffusiophoretic mobility $\hat{M}$ relates to the dimensional diffusiophoretic mobility M via

$$\hat{M} = \frac{\hat{U}}{\alpha} = \frac{e^2 \eta}{\varepsilon k^2 T^2} M. \quad (10)$$

To solve eqn (8) and (9) in a finite computational domain, it again requires transforming the far-field boundary conditions at $\hat{r} \to \infty$ to ones at $\hat{r} = \hat{R}$. First, in the asymptotic limit of

a vanishing electric potential at a sufficiently large $\hat{R}$, the far-field boundary condition for $\hat{\psi}_i{}^1$ that was at $\hat{r} \to \infty$ is transformed to be

$$2\widehat{\Psi}_i{}^1 + \hat{R}\frac{\mathrm{d}\widehat{\Psi}_i{}^1}{\mathrm{d}\hat{r}} = 3\left(\beta - \frac{1}{z_i}\right)\hat{R} \text{ at } \hat{r} = \hat{R}. \quad (11)$$

Second, the net hydrodynamic and electric forces are zero on the large sphere of radius $\hat{R}$ that encloses a freely suspended colloid. A sufficiently large $\hat{R}$ guarantees that the sphere is electric force-free.[50,63–65] Thus, the constraint reduces to that the sphere is hydrodynamic force-free: $\hat{F} = 2\pi\hat{R}^2 \int_0^\pi \hat{\sigma}\cdot n \sin\theta \,\mathrm{d}\theta - 2\pi\gamma^2 \int_0^\pi \int_1^{\hat{R}}(\hat{u} + \hat{U})\hat{r}^2 \sin\theta \,\mathrm{d}\hat{r}\,\mathrm{d}\theta = \mathbf{0}$, where $\hat{\sigma} = -\hat{p}I + \widehat{\nabla}\hat{u} + (\widehat{\nabla}\hat{u})^T$ is the Newtonian stress tensor and I is the identity tensor. Rearranging eqn (9) at $\hat{r} = \hat{R}$ with the hydrodynamic force-free condition yields

$$\lambda\hat{R}\frac{\mathrm{d}^2\hat{h}}{\mathrm{d}\hat{r}^2} - \left(4\gamma^3 + 3\gamma^3\hat{R}^3 + 9\gamma^2\hat{R}^2 + 18\gamma\hat{R} + 18\right)\hat{h}$$
$$+ \left[-6\gamma^2 + 3\gamma^3\hat{R}^4 + 9\gamma^2\hat{R}^3 + 18\gamma\hat{R}^2 - 2(\gamma^3 - 9)\hat{R}\right]\frac{\mathrm{d}\hat{h}}{\mathrm{d}\hat{r}} = 0, \quad (12)$$

$$-9\gamma\left(\gamma^2\hat{R}^2 + 2\gamma\hat{R} + 2\right)\hat{h} + 3\gamma(-2\gamma^2 + 3\gamma^2\hat{R}^3 + 6\gamma\hat{R}^2 + 6\hat{R})\frac{\mathrm{d}\hat{h}}{\mathrm{d}\hat{r}}$$
$$+ \lambda\left[\hat{R}\frac{\mathrm{d}^3\hat{h}}{\mathrm{d}\hat{r}^3} + \left(\gamma\hat{R} + 4\right)\frac{\mathrm{d}^2\hat{h}}{\mathrm{d}\hat{r}^2}\right] = 0, \quad (13)$$

$$\hat{M} = \left[\frac{6\left(\gamma^2\hat{R}^2 + 2\gamma\hat{R} + 2\right)}{\lambda}\right]\hat{h} + \left[\frac{6\hat{R}\left(\gamma\hat{R} + 1\right)}{\lambda}\right]\frac{\mathrm{d}\hat{h}}{\mathrm{d}\hat{r}}, \quad (14)$$

where $\lambda = -2\gamma^2 + 3\gamma^2\hat{R}^3 + 9\gamma\hat{R}^2 + 9\hat{R}$. In sum, we solve eqn (8) and (9) for $\hat{h}$ and $\hat{\psi}_i{}^1$ subject to the boundary conditions $\mathrm{d}\hat{\psi}_i{}^1/\mathrm{d}\hat{r} = 0$, $\hat{h} = 0$, and $\mathrm{d}\hat{h}/\mathrm{d}\hat{r} = 0$ at $\hat{r} = 1$, in addition to the boundary conditions (11) to (13) at $\hat{r} = \hat{R}$, using the solver *NDSolve* in Wolfram Mathematica and the solver *bvp4c* in MATLAB. We obtain the diffusiophoretic mobility from eqn (14). We have validated the present model by recovering results from prior work. Details are presented in Appendix A.

3 Results and discussion

Current knowledge of diffusiophoresis in porous media is limited to porous media saturated with a valence symmetric electrolyte.[17,50–55] In this section, we compute and discuss novel results diffusiophoresis in porous media saturated with a valence asymmetric electrolyte, in addition to a mixture of valence symmetric and asymmetric electrolytes. Model inputs taken from typical experiments are listed in Table 1. The zeta potential $\zeta \in [-100, 100]$ mV corresponds to $\hat{\zeta} \in [-4, 4]$. The porous medium pore diameter is at least about 1.5 times the colloid diameter, which allows the passage of the colloid. In Section 3.1, we demonstrate the first and the second key findings of this work. Namely, in the same electrolyte, lowering the permeability of the porous medium significantly weakens the colloid diffusiophoretic motion. Also, surprisingly, in an valence asymmetric electrolyte, diffusiophoresis in a denser porous medium can be stronger than that in a less dense porous medium saturated with a valence symmetric electrolyte. In Section 3.2, we demonstrate the third key finding of this work. Namely, in a mixture of electrolytes, not just the magnitude but also the direction of the colloid motion can change by varying the mixture composition.

3.1 Diffusiophoresis in porous media saturated with a valence asymmetric electrolyte

Let us first examine diffusiophoresis in porous media saturated with a AlCl₃ solution. Fig. 2(a) shows the non-dimensionalized diffusiophoretic mobility $\hat{M}$ versus the non-dimensionalized colloid surface potential $\hat{\zeta}$. The ionic strength of the solution is $I = 0.25$ mM. Let us first focus on the black line with $l/a \gg 1$, which corresponds to an infinitely permeable porous media, *i.e.*, an electrolyte solution in the absence of porous media. Here, the first observation is that for a negatively charged colloid $\hat{M}$ is positive, whereas for a positively charged colloid $\hat{M}$ is negative. This is consistent with the classical understanding of diffusiophoresis as follows.[1–4] Let us first consider a negatively charged colloid as shown in Fig. 2(b). A negative β implies that the induced electric field E is pointing in the negative z-direction. The field E drives positive counterions to the left and generates an electroosmotic flow in the same direction, causing the colloid to undergo electrophoresis to the right. Meanwhile, the osmotic pressure gradient induced by the electrolyte concentration gradient generates a chemiosmotic flow to the left, causing the colloid to undergo chemiphoresis to the right. Since diffusiophoresis is the sum of electrophoresis and chemiphoresis, diffusiophoresis acts in the positive z-direction and $\hat{M}$ is positive. In contrast, for a positively charged colloid as shown in Fig. 2(c), electrophoresis which acts to the left outweighs chemiphoresis which acts to the right. This results in

Table 1 Input parameters for computation

| Parameters	Values	Ion diffusivities[66]	Values
Colloid radius (a)[17,20,52]	100 nm	Potassium (D_{K^+})	1.96×10^{-9} m² s⁻¹
Ionic strength (I)[17,20]	[0.25, 1] mM	Sodium (D_{Na^+})	1.33×10^{-9} m² s⁻¹
Screening length (l)[17,20,67,68]	$\geq$50 nm	Barium $(D_{\mathrm{Ba}^{2+}})$	0.847×10^{-9} m² s⁻¹
Temperature (T)	298 K	Magnesium $(D_{\mathrm{Mg}^{2+}})$	0.706×10^{-9} m² s⁻¹
Permittivity (ε)	6.95×10^{-10} F m⁻¹	Aluminum $(D_{\mathrm{Al}^{3+}})$	0.541×10^{-9} m² s⁻¹
Dynamic viscosity (η)	0.891×10^{-3} kg m⁻¹ s⁻¹	Lanthanum $(D_{\mathrm{La}^{3+}})$	0.619×10^{-9} m² s⁻¹
Surface potential (ζ)[17,20,52,58,69–73]	[−100, 100] mV	Chloride (D_{Cl^-})	2.03×10^{-9} m² s⁻¹

diffusiophoresis acting in the negative z-direction and $\hat{M}$ is negative.

The second observation of the black line in Fig. 2(a) is that for a negatively charged colloid the magnitude of $\hat{M}$ experiences a decay at $\hat{\zeta} \leq 1$, whereas for a positively charged colloid the magnitude of $\hat{M}$ is monotonically increasing. This can be understood by examining the ionic transport between the two cases. Let us first consider a negatively charged colloid by referring to Fig. 2(b). Both the electroosmotic and chemiosmotic flow are transporting positive counterions downstream to the colloid to the left. Due to coulombic attraction, these counterions will slow down the colloid motion that is to the right.[4,63] The stronger the colloid's charge, the stronger this slowing-down effect to the colloid. Therefore, $\hat{M}$ decays as $\hat{\zeta}$ becomes more negative. Next, let us consider a positively charged colloid by referring to Fig. 2(c). In contrast to Fig. 2(b), in Fig. 2(c) only the electroosmotic flow is transporting negative counterions downstream to the colloid to the right, whereas the chemiosmotic flow is transporting counterions upstream to the colloid to the left. As a result, the slowing-down effect to the colloid due to coulombic attraction between the counterions and the colloid is weak. Therefore, the magnitude of $\hat{M}$ does not experience a decay but grows monotonically.

The first key finding of this work arises from an overview of Fig. 2(a), where decreasing l/a decreases the magnitude of $\hat{M}$ significantly. For example, at $\hat{\zeta} = 2$, decreasing l/a (from black to green line) decreases the magnitude of $\hat{M}$ from 0.459 to 0.298. Physically, decreasing l/a implies decreasing the permeability of the porous medium to the transport of the electrolyte and the colloid. That is, the presence of porous media is to weaken the magnitude of diffusioosmosis (and its constituting electroosmosis and chemiosmosis), and therefore the magnitude of the resulting diffusiophoresis (and its constituting electrophoresis and chemiphoresis). As the permeability decreases, the hydrodynamic drag to the electrolyte and the colloid increases, and therefore $\hat{M}$ decreases. This key finding is consistent with the fundamental nature of porous media in weakening hydrodynamics.[56,57] Also, this key finding and the two observations in the previous paragraphs hold in a lower valence, valence asymmetric electrolyte BaCl$_2$ as shown in Fig. 2(d) and in a valence symmetric electrolyte NaCl as shown in Fig. 2(e).

Next, let us turn to Fig. 3. We consider a porous medium with $l = 75$ nm. In three difference cases, the porous medium is saturated with three different electrolyte solutions, AlCl$_3$, BaCl$_2$, and NaCl. The ionic strength of the three solutions are the same as $I = 0.25$ mM. The third observation is that, for a negatively
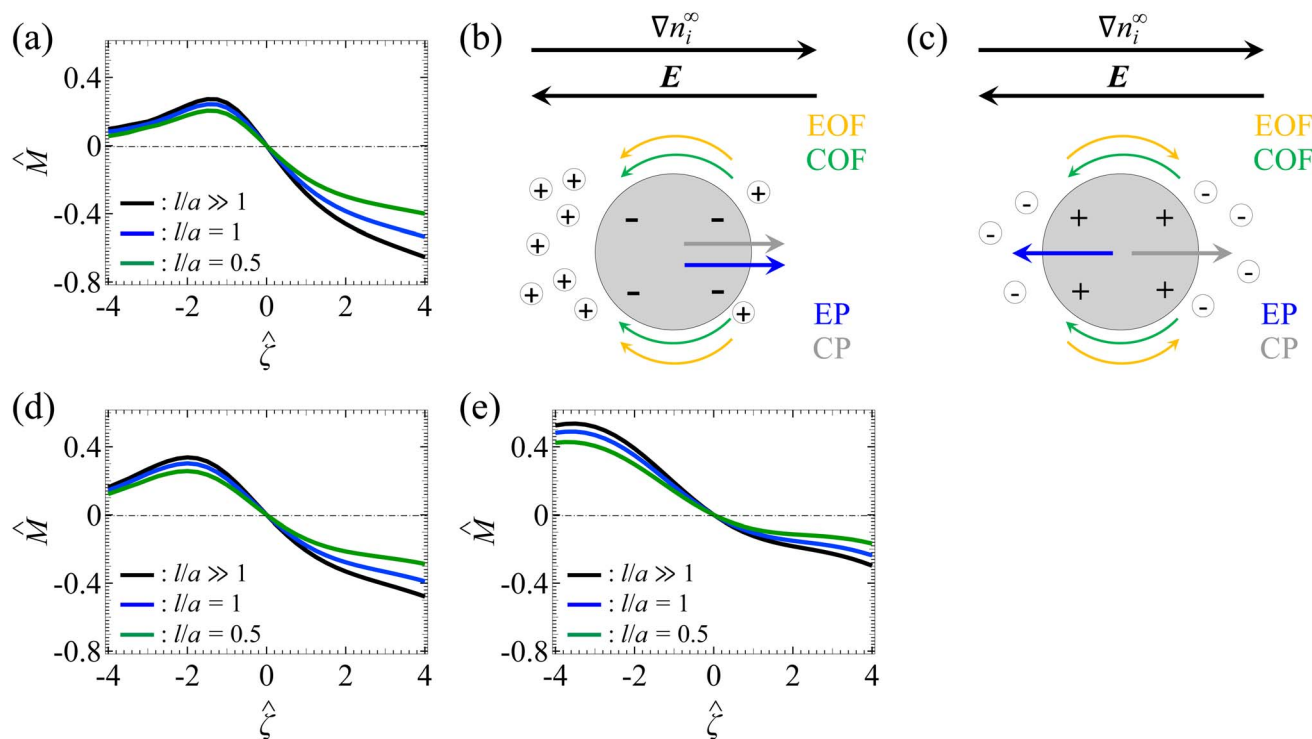
Fig. 2 (a) The non-dimensionalized diffusiophoretic mobility $\hat{M}$ versus the non-dimensionalized colloid surface potential $\hat{\zeta}$ in different porous media saturated with a AlCl$_3$ solution of ionic strength $I = 0.25$ mM. Black line: an electrolyte solution in the absence of porous media (the ratio of the screening length to the colloid radius $l/a \gg 1$). Blue line: a less dense porous medium ($l/a = 1$). Green line: a denser porous medium ($l/a = 0.5$). (b) A negatively charged colloid undergoing diffusiophoresis moving in the positive z-direction (to the right). The induced electric field $\boldsymbol{E}$ points to the negative z-direction. Both the electroosmotic flow (EOF) and chemiosmotic flow (COF) transport ions in the negative z-direction. Both electrophoresis (EP) and chemiphoresis (CP) in diffusiophoresis move the colloid in the positive z-direction. (c) A positively charged colloid undergoing diffusiophoresis moving in the negative z-direction (to the left). The EOF transports ions in the positive z-direction and the COF transports ions in the negative z-direction. CP is outweighed by EP which acts in the negative z-direction. (d) $\hat{M}$ versus $\hat{\zeta}$ in different porous media saturated with a BaCl$_2$ solution. (e) $\hat{M}$ versus $\hat{\zeta}$ in different porous media saturated with a NaCl solution. The color scheme and the ionic strength of (d) and (e) are the same as (a).
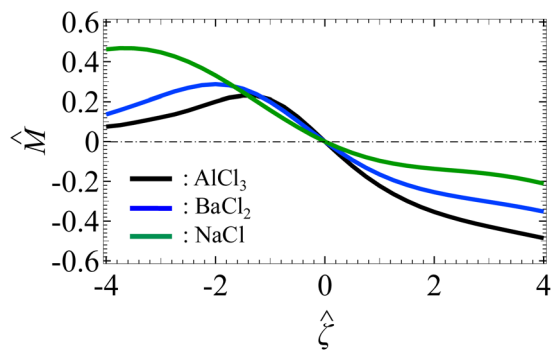
Fig. 3 The non-dimensionalized diffusiophoretic mobility $\hat{M}$ *versus* the non-dimensionalized colloid surface potential $\hat{\zeta}$ in the same porous media (the ratio of the screening length to the colloid radius $l/a = 0.75$) saturated with different electrolyte solutions of ionic strength $I = 0.25$ mM. Black line: AlCl$_3$. Blue line: BaCl$_2$. Green line: NaCl.

charged colloid, the decay in the diffusiophoretic mobility $\hat{M}$ occurs at a lower colloid surface potential $\hat{\zeta}$ in a higher valence electrolyte than in a lower valence electrolyte. For example, the decay in $\hat{M}$ for AlCl$_3$ (black line) occurs at $\hat{\zeta} \leq -1$, whereas the decay for NaCl (green line) occurs at $\hat{\zeta} \leq -3.5$. This can be understood by recalling the explanation for the second observation. Specifically, the decay is due to the coulombic attraction between the colloid and the downstream counterions. For AlCl$_3$, the counterions are Al^{3+}, which have a higher charge density than the counterions Na$^+$ of NaCl. Hence, at the same $\hat{\zeta}$, the coulombic attraction between the colloid and Al^{3+} is stronger than that between the colloid and Na$^+$. As a result, the decay in $\hat{M}$ occurs at a weaker $\hat{\zeta}$ for AlCl$_3$.

The fourth observation is from the range of a positive $\hat{\zeta}$ in Fig. 3, where $\hat{M}$ can be increasingly enhanced by a more valence asymmetric electrolyte. The enhancement in $\hat{M}$ is significant. For example, at $\hat{\zeta} = 2$, $\hat{M}$ for NaCl is -0.137 (green line). In a BaCl$_2$ solution, $\hat{M}$ has a 86% increase and equals -0.254 (blue line). In a AlCl$_3$ solution, $\hat{M}$ has a 158% increase and equals -0.354 (black line). As noted in the first observation, the
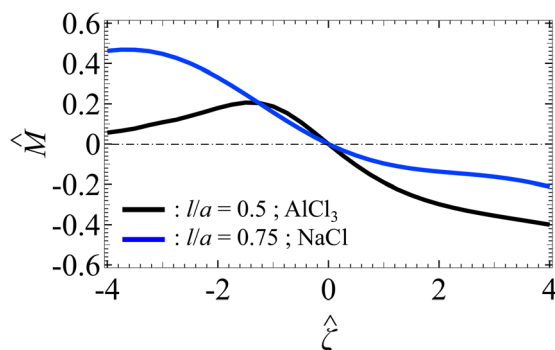
electrophoretic component of diffusiophoresis dominates for a positively charged colloid. The driving force for electrophoresis is the induced electric field $\boldsymbol{E} = (kT/e)\beta\boldsymbol{G}$, which is proportional to the ion diffusivity ratio β. Thus, as the magnitude of β increases from $|\beta| = 0.207$ (NaCl) to $|\beta| = 0.318$ (BaCl$_2$) and $|\beta| = 0.408$ (AlCl$_3$), the magnitude of $\hat{M}$ increases.

Next, let us turn to Fig. 4. The black line denotes a denser porous medium ($l/a = 0.5$) saturated with a AlCl$_3$ solution and the blue line denotes a less dense porous medium ($l/a = 0.75$) saturated with a NaCl solution. The solution ionic strength $I = 0.25$ mM is the same in the two cases. Here, the second key finding of this work is that the magnitude of the diffusiophoretic mobility $\hat{M}$ in a denser porous medium can be stronger than that in a less dense porous medium. For example, for a positive colloid surface potential $\hat{\zeta}$, the magnitude of the black line is larger than that of the blue line. This is a rather surprising and non-intuitive result, as one may expect that the colloid movement in a denser porous medium is always weaker than that in a less dense porous medium due to the stronger hydrodynamic drag to the fluid and the colloid. However, results here show that, by employing a valence asymmetric electrolyte, diffusiophoresis in a denser porous medium can be much stronger than that in a less dense porous medium saturated with a valence symmetric electrolyte. Physically, this is because the enhancement to the electrophoretic component of diffusiophoresis by the valence asymmetric electrolyte outweighs the hydrodynamic drag due to the porous media. This finding offers new insights into using valence asymmetric electrolyte to generate strong diffusiophoresis in porous media.

3.2 Diffusiophoresis in porous media saturated with a mixture of valence symmetric and asymmetric electrolytes

Let us examine diffusiophoresis in porous media saturated with solution mixtures of p molar of KCl and q molar of LaCl$_3$ with different compositions $f = q/(p + q)$, where $f \in [0, 1]$ with $f = 0$ and $f = 1$ representing a pure KCl solution and a pure LaCl$_3$ solution, respectively. Fig. 5(a) shows the diffusiophoretic mobility $\hat{M}$ *versus* the colloid surface potential $\hat{\zeta}$. The screening length is $l = 75$ nm and the ionic strength of the solution is $I = 1$ mM. Let us first focus on the black and the red line with $f = 1$ and $f = 0$, respectively. The first observation is that the variation of $\hat{M}$ *versus* $\hat{\zeta}$ in a pure LaCl$_3$ solution ($f = 1$; black line) is qualitatively different from that in a pure KCl solution ($f = 0$; red line). Specifically, in a pure LaCl$_3$ solution, $\hat{M}$ is positive for a negative $\hat{\zeta}$ and is negative for a positive $\hat{\zeta}$. This follows the same trend and explanation as for AlCl$_3$ in the first observation in Section 3.1 and is not repeated here. In contrast, in a pure KCl solution, $\hat{M}$ is positive regardless of the sign of $\hat{\zeta}$. This is understood by noting the very small value $\beta = -0.0188$, which reflects the negligibly small electrophoretic contribution in diffusiophoresis. Hence, the colloid undergoes diffusiophoresis chiefly due to chemiphoresis that drives the colloid in the positive z-direction and thus $\hat{M}$ is positive.

The third key finding of this work is that varying the mixture composition f can change not just the magnitude of the colloid diffusiophoretic motion drastically, but also qualitatively its
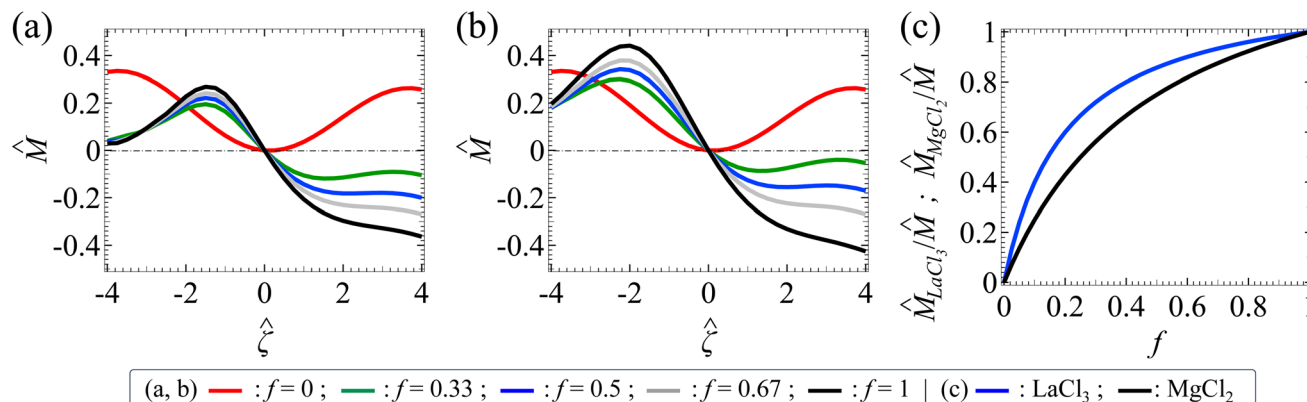

Fig. 4 The non-dimensionalized diffusiophoretic mobility $\hat{M}$ *versus* the non-dimensionalized colloid surface potential $\hat{\zeta}$ in different porous media saturated with different electrolyte solutions of ionic strength $I = 0.25$ mM. Black line: a denser porous medium (the ratio of the screening length to the colloid radius $l/a = 0.5$) saturated with a AlCl$_3$ solution. Blue line: a less dense porous medium ($l/a = 0.75$) saturated with a NaCl solution.

Fig. 5 (a) The non-dimensionalized diffusiophoretic mobility $\hat{M}$ versus the non-dimensionalized colloid surface potential $\hat{\zeta}$ in the same porous media (the ratio of the screening length to the colloid radius $l/a = 0.75$) saturated with solution mixtures of p molar of KCl and q molar of LaCl$_3$ with different compositions $f = q/(p + q)$. The solution ionic strength $I = 1$ mM. Red line: $f = 0$. Green line: $f = 0.33$. Blue line: $f = 0.5$. Grey line: $f = 0.67$. Black line: $f = 1$. (b) $\hat{M}$ versus $\hat{\zeta}$ in the same porous media ($l/a = 0.75$) saturated with solution mixtures of p molar of KCl and q molar of MgCl$_2$ with different compositions $f = q/(p + q)$. The color scheme and the ionic strength are the same as (a). (c) The ratio of the contribution to the mobility by the asymmetric electrolyte to that by the mixture $\hat{M}_{\text{LaCl}_3}/\hat{M}$ and $\hat{M}_{\text{MgCl}_2}/\hat{M}$ versus f. Blue line: $\hat{M}_{\text{LaCl}_3}/\hat{M}$. Black line: $\hat{M}_{\text{MgCl}_2}/\hat{M}$.

direction; the latter is reflected from the sign change of $\hat{M}$ for a fixed positive $\hat{\zeta}$ as f increases. In a mixture of electrolytes, $\hat{M}$ is not simply the superposition nor the weighted average of the contributions from its individual electrolyte. For example, in Fig. 5(a) at $\hat{\zeta} = 3$, $\hat{M}_{f=0} = 0.240$ (red line) and $\hat{M}_{f=1} = -0.328$ (black line), but $\hat{M}_{f=0.5} = -0.179$ (blue line) $\neq (\hat{M}_{f=0} + \hat{M}_{f=1})/2$. In fact, $\hat{M}$ depends nonlinearly on f. This is because $\hat{M}$ is a result of the nonlinearly coupled Poisson–Nernst–Planck and Brinkman eqn (1)–(3). Because of this intricate coupling, $\hat{M}$ can vary non-monotonically with f. For example, at $\hat{\zeta} = -2.8$, $\hat{M}_{f=0} = 0.283$ (red line); as f increases, $\hat{M}$ first decreases and then increases. In the special case at $\hat{\zeta} = -2.4$, $\hat{M}_{f=0}$ (red line) can even be identical to $\hat{M}_{f=1}$ (black line), meaning that a colloid undergoes the same diffusiophoretic motion regardless of the electrolyte identity. These observations are not restricted to a KCl/LaCl$_3$ mixture but is general to other electrolyte mixtures. For example, Fig. 5(b) shows a similar set of diffusiophoretic response in a KCl/MgCl$_2$ mixture as in Fig. 5(a). These observations underline the importance of this work to solve the coupled Poisson–Nernst–Planck–Brinkman equations to predict diffusiophoresis.

A scaling analysis illustrates that the nonlinearity between $\hat{M}$ and f depends on the ion valence z. First, referring to the far-field boundary condition below eqn (9), $\hat{M} \sim \hat{h}$. Further, from eqn (9), $\hat{h} \sim \sum_{i=1}^{N} z_i^2 \hat{n}_i^0 \sim \sum_{i=1}^{N} z_i^2 \hat{n}_i^\infty \sim \hat{I}$, where $\hat{I}$ is the non-dimensionalized mixture ionic strength. Combining these relations, $\hat{M} \sim \hat{I}$. Second, recall that $f = q/(p + q)$. Stoichiometry requires that the ionic strength of KCl is $I_{\text{KCl}} = (1/2)(z_{\text{K}^+}^2 p + z_{\text{Cl}^-}^2 p)$ M $= p$ M, with $z_{\text{K}^+} = -z_{\text{Cl}^-} = 1$. The ionic strength of LaCl$_3$ is $I_{\text{LaCl}_3} = (1/2)(z_{\text{La}^{3+}}^2 q + z_{\text{Cl}^-}^2 q)$ M $= 6q$ M, with $z_{\text{La}^{3+}} = 3$ and $z_{\text{Cl}^-} = -1$. Note that I_{LaCl_3} increases nonlinearly with an increase in the ion valence $z_{\text{La}^{3+}}^2$. Thus, $I = I_{\text{KCl}} + I_{\text{LaCl}_3} = p + 6q$ M. Upon non-dimensionalization, $\hat{I}_{\text{LaCl}_3} = 6\hat{q}$ and $\hat{I} = \hat{q}(5f + 1)/f$. Recall that $\hat{M} \sim \hat{I}$, thus $\hat{M}_{\text{LaCl}_3} \sim \hat{I}_{\text{LaCl}_3}$, where $\hat{M}_{\text{LaCl}_3}$ is the

contribution of LaCl$_3$ to the mobility of the mixture $\hat{M}$. Thus, it is established that

$$\frac{\hat{M}_{\text{LaCl}_3}}{\hat{M}} = \frac{6f}{(1 + 5f)}, \tag{15}$$

$$\frac{\hat{M}_{\text{MgCl}_2}}{\hat{M}} = \frac{3f}{(1 + 2f)}, \tag{16}$$

where eqn (16) is obtained for a KCl/MgCl$_2$ mixture following a similar procedure as eqn (13). Fig. 5(c) shows the nonlinear relations of $\hat{M}_{\text{LaCl}_3}/\hat{M}$ and $\hat{M}_{\text{MgCl}_2}/\hat{M}$ to f. Note that $\hat{M}_{\text{LaCl}_3}/\hat{M}$ (blue line) shows a stronger increase than $\hat{M}_{\text{MgCl}_2}/\hat{M}$ (black line) at the same f. This is because the nonlinearity in the ion valence for $z_{\text{La}^{3+}}^2 = 9$ is stronger than that for $z_{\text{Mg}^{2+}}^2 = 4$. This explains why in Fig. 5(a) and (b) the sensitivity of $\hat{M}$ to a change in f in a KCl/LaCl$_3$ mixture is stronger than that in a KCl/MgCl$_2$ mixture.

Before closing, we demonstrate the generality of the first two key findings of this work, which were demonstrated in Section 3.1 with a valence asymmetric electrolyte, in an electrolyte mixture. First, recall the first key finding that the magnitude of diffusiophoresis weakens significantly as the porous medium permeability decreases. Fig. 6(a) shows the diffusiophoretic mobility $\hat{M}$ versus the colloid surface potential $\hat{\zeta}$ in different porous media saturated with a KCl/LaCl$_3$ mixture of composition $f = 0.5$. The first key finding is confirmed that the magnitude of $\hat{M}$ decreases substantially as l/a decreases (from black to green line). In fact, the first key finding holds not just in a mixture of two electrolytes. Fig. 6(b) shows $\hat{M}$ versus $\hat{\zeta}$ in different porous media saturated with a phosphate-buffered saline (PBS) solution, which is a mixture of NaCl, KCl, Na$_2$HPO$_4$, and KH$_2$PO$_4$. The detailed ionic composition of the PBS solution is given in Appendix B. Again, the first key finding is confirmed by the decreasing magnitude of $\hat{M}$ with decreasing l/a (from black to green line).
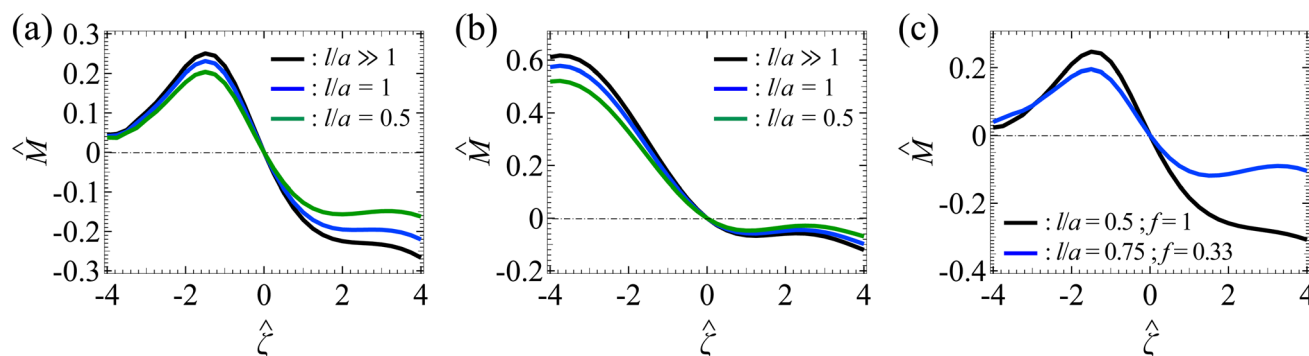
Fig. 6 (a) The non-dimensionalized diffusiophoretic mobility $\hat{M}$ versus the non-dimensionalized colloid surface potential $\hat{\zeta}$ in different porous media saturated with a solution mixture of p molar of KCl and q molar of LaCl$_3$ with a composition $f = q/(p+q) = 0.5$. The solution ionic strength $I = 1$ mM. Black line: an electrolyte solution in the absence of porous media (the ratio of the screening length to the colloid radius $l/a \gg$ 1). Blue line: a less dense porous medium $l/a = 1$. Green line: a denser porous medium $l/a = 0.5$. (b) $\hat{M}$ versus $\hat{\zeta}$ in different porous media saturated with a phosphate-buffered saline (PBS) solution. The color scheme and the ionic strength are the same as (a). (c) $\hat{M}$ versus $\hat{\zeta}$ in different porous media saturated with different KCl/LaCl$_3$ mixtures of $I = 1$ mM. Black line: a denser porous medium saturated with a higher fraction of valence asymmetric electrolyte $l/a = 0.5$ and $f = 1$. Blue line: a less dense porous medium saturated with a lower fraction of valence asymmetric electrolyte $l/a = 0.75$ and $f = 0.33$.

Lastly, recall the second key finding that, with a valence asymmetric electrolyte, diffusiophoresis in a denser porous medium can be stronger than diffusiophoresis in a less dense porous medium saturated with a valence symmetric electrolyte. Fig. 6(c) shows $\hat{M}$ versus $\hat{\zeta}$ in different porous media saturated with different KCl/LaCl$_3$ mixtures. The black line corresponds to a denser porous medium ($l/a = 0.5$) saturated with a mixture with a higher fraction of LaCl$_3$ ($f = 1$), whereas the blue line corresponds to a less dense porous medium ($l/a = 0.75$) saturated with a mixture with a lower fraction of LaCl$_3$ ($f = 0.33$). The second key finding is confirmed by observing that for positive $\hat{\zeta}$ the magnitude of $\hat{M}$ of the black line can indeed be larger than that of the blue line. In sum, these results underline the novelty of this work and the importance of leveraging valence asymmetric electrolytes and electrolyte mixtures to achieve richer responses in diffusiophoresis in porous media.

4 Conclusions

In this work, we have developed a predictive model for diffusiophoresis in porous media saturated with a general mixture of electrolytes. Prior models have focused either on diffusiophoresis in a mixture of electrolytes in the absence of porous media,[19,42–44,46–49] or diffusiophoresis in porous media saturated with a valence symmetric electrolyte.[17,50–55] The present model is novel in that it accounts for the coupled effects of porous media and electrolyte mixtures. We have computed the diffusiophoretic mobilities in porous media saturated with a valence asymmetric electrolyte as well as in porous media saturated with a mixture of valence symmetric and asymmetric electrolytes. We summarize the three key findings below.

The first key finding of this work is that, in the same electrolyte solution, decreasing the porous medium permeability weakens the colloid diffusiophoretic motion significantly. This is consistent with the fundamental nature of porous media which provides a larger hydrodynamic hindrance to the colloid and the suspending fluid, and thus, weakens diffusiophoresis.

This key finding is consistent with the same conclusion drawn in prior work for diffusiophoresis in porous media saturated with a valence symmetric electrolyte.[17,50–52] Here, we have generalized this key finding to diffusiophoresis in porous media saturated with a valence asymmetric electrolyte and a general mixture of electrolytes.

The second key finding is that, by utilizing a valence asymmetric electrolyte, diffusiophoresis in a denser porous medium can be stronger than that in a less dense porous medium saturated with a valence symmetric electrolyte. This is contrary to what one might expect that diffusiophoresis in a denser porous medium is always weaker. In fact, this surprising result is due to the fact that valence asymmetric electrolyte can generate a stronger electrophoretic motion of the colloid, which outweighs the hydrodynamic drag due to the porous medium. We have further generalized this key finding by showing that diffusiophoresis in a denser porous medium saturated with a mixture of higher fraction of asymmetric electrolyte can be stronger than that in a less dense porous medium saturated with a mixture of lower fraction of asymmetric electrolyte.

The third key finding is that varying the mixture composition can change not only the magnitude of the diffusiophoretic motion significantly, but also qualitatively its direction. The diffusiophoretic mobility in an electrolyte mixture is not simply the superposition nor the weighted average of the contributions from its individual electrolyte. This is because diffusiophoresis is governed by the nonlinearly coupled Poisson–Nernst–Planck–Brinkman equations. This underlines the value of the present work to determine the colloid diffusiophoretic motion by solving the coupled governing equations. Together, the present model and these key findings will enable fundamental understanding of diffusiophoresis in porous media and predict a richer set of diffusiophoresis responses in the presence of an electrolyte mixture.

Data availability

All data that supports this study is included in this article.

Conflicts of interest

There are no conflicts of interest to declare.

Appendices

Appendix A: Model validations

We validate the present model by recovering results from prior work. First, Fig. 7 shows that the present model recovers Fig. 4 in Sambamoorthy and Chu,[50] for diffusiophoresis in different
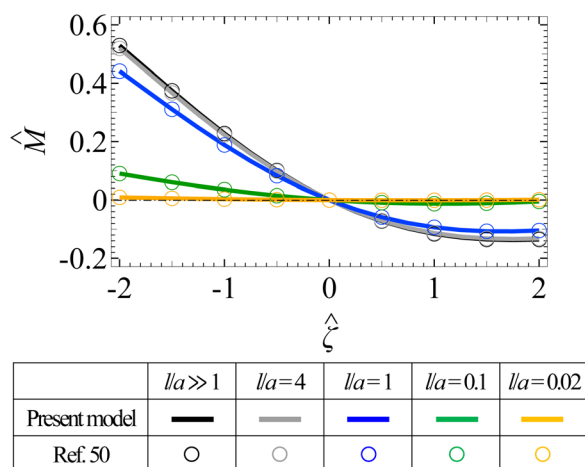

	$l/a \gg 1$	$l/a = 4$	$l/a = 1$	$l/a = 0.1$	$l/a = 0.02$
Present model	▬	▬	▬	▬	▬
Ref. 50	○	○	○	○	○

Fig. 7 The non-dimensionalized diffusiophoretic mobility $\hat{M}$ versus the non-dimensionalized colloid surface potential $\hat{\zeta}$ in different porous media saturated with a NaCl solution with the Debye–Huckel approximation. Lines: predictions by the present model. Symbols: predictions by Sambamoorthy and Chu.[50] Black: the ratio of the screening length to the colloid radius $l/a \gg 1$. Grey: $l/a = 4$. Blue: $l/a = 1$. Green: $l/a = 0.1$. Orange: $l/a = 0.02$.
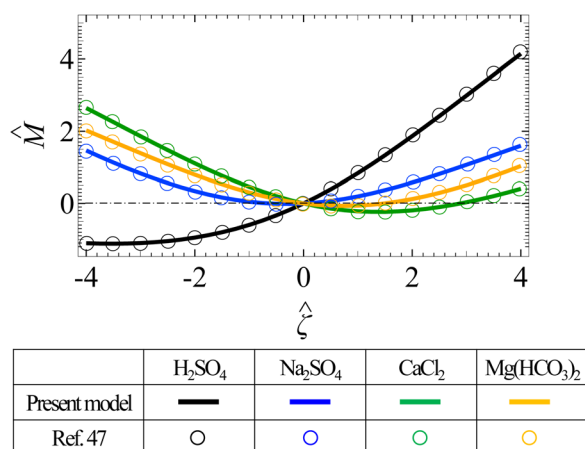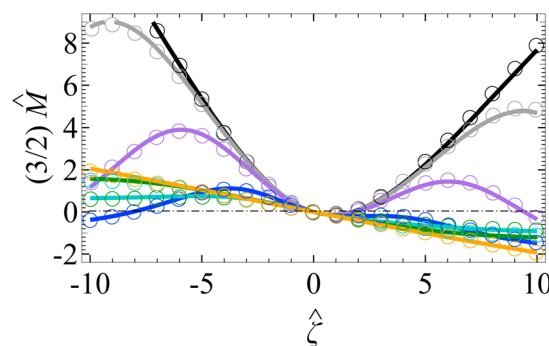

	NaCl	KCl	NH$_4$F
Present model	▬	▬	▬
Ref. 1	○	○	○

Fig. 8 The non-dimensionalized diffusiophoretic mobility $\hat{M}$ versus the non-dimensionalized colloid surface potential $\hat{\zeta}$ in different valence asymmetric electrolyte solutions in the limit of a thin electric double layer (the ratio of the colloid radius to the Debye length $\hat{\kappa} \gg 1$) and in the absence of porous media (the ratio of the screening length to the colloid radius $l/a \gg 1$). Lines: predictions by the present model. Symbols: predictions by Gupta et al.[47] Black: H$_2$SO$_4$. Blue: Na$_2$SO$_4$. Green: CaCl$_2$. Orange: Mg(HCO$_3$)$_2$.

	$\hat{\kappa} \gg 1$	$\hat{\kappa} = 1000$	$\hat{\kappa} = 10$	$\hat{\kappa} = 10$
Present model	▬	▬	▬	▬
Ref. 65	○	○	○	○
	$\hat{\kappa} = 1$	$\hat{\kappa} = 0.1$	$\hat{\kappa} = 0$	
Present model	▬	▬	▬	
Ref. 65	○	○	○	

Fig. 9 The non-dimensionalized diffusiophoretic mobility $(3/2)\hat{M}$ versus the non-dimensionalized colloid surface potential $\hat{\zeta}$ in a NaCl solution in the absence of porous media (the ratio of the screening length to the colloid radius $l/a \gg 1$). Lines: predictions by the present model. Symbols: predictions by Prieve and Roman.[65] Black: the ratio of the colloid radius to the Debye length $\hat{\kappa} \gg 1$. Grey: $\hat{\kappa} = 1000$. Purple: $\hat{\kappa} = 100$. Blue: $\hat{\kappa} = 10$. Cyan: $\hat{\kappa} = 1$. Green: $\hat{\kappa} = 0.1$. Orange: $\hat{\kappa} = 0$.

porous media saturated with a NaCl solution. Second, Fig. 8 shows that the present model recovers Fig. 3 in Gupta et al.,[47] for diffusiophoresis in different valence asymmetric electrolyte solutions in the limit of a thin electric double layer and in the absence of porous media. Here, the diffusiophoresis results have the same magnitude and an opposite sign as the
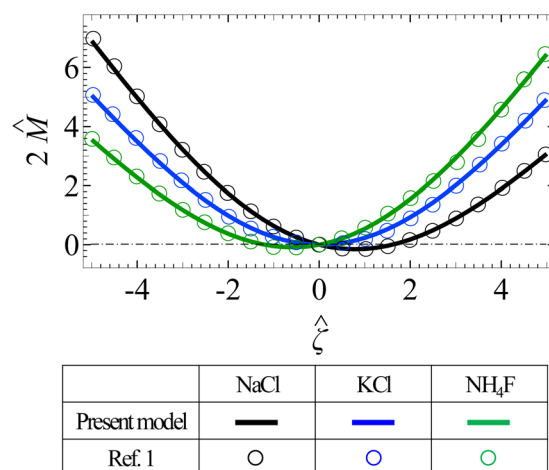

	H$_2$SO$_4$	Na$_2$SO$_4$	CaCl$_2$	Mg(HCO$_3$)$_2$
Present model	▬	▬	▬	▬
Ref. 47	○	○	○	○

Fig. 10 The non-dimensionalized diffusiophoretic mobility $2\hat{M}$ versus the non-dimensionalized colloid surface potential $\hat{\zeta}$ in different valence symmetric electrolyte solutions in the limit of a thin electric double layer (the ratio of the colloid radius to the Debye length $\hat{\kappa} \gg 1$) and in the absence of porous media (the ratio of the screening length to the colloid radius $l/a \gg 1$). Lines: predictions by the present model. Symbols: predictions by Prieve et al.[1] Black: NaCl. Blue: KCl. Green: NH$_4$F.

diffusioosmosis results in Gupta et al.,[47] since diffusiophoresis is the exact opposite of diffusioosmosis in the limit of a thin electric double layer. Third, Fig. 9 shows that the present model recovers Fig. 9 in Prieve and Roman,[65] for diffusiophoresis in a NaCl solution in the absence of porous media. Lastly, Fig. 10 shows that the present model recovers Fig. 4 in Prieve et al.,[1] for diffusiophoresis in different valence symmetric electrolyte solutions in the limit of a thin electric double layer and in the absence of porous media.

Appendix B: Ionic composition of phosphate-buffered saline solution

A $1\times$ phosphate-buffered saline (PBS) solution comprises 137 mM NaCl, 2.7 mM KCl, 10 mM Na_2HPO_4, and 1.8 mM KH_2PO_4. From dissociation, there are 157 mM Na^+, 139.7 mM Cl^-, 4.5 mM K^+, 10 mM HPO_4^{2-}, and 1.8 mM $H_2PO_4^-$. Dihydrogen phosphate ion $H_2PO_4^-$ and monohydrogen phosphate ions HPO_4^{2-} have a chemical equilibrium, $H_2PO_4^- \rightleftharpoons H^+ + HPO_4^{2-}$, with an equilibrium constant of $10^{-4.21}$ mM and diffusivities $D_{HPO_4^{2-}} = 0.439 \times 10^{-9}$ m^2 s^{-1} and $D_{H_2PO_4^-} = 0.879 \times 10^{-9}$ m^2 s^{-1}.[66,74] Thus, there is 1.11×10^{-5} mM H^+, which is negligible compared to the five dominant species, namely, Na^+, K^+, Cl^-, HPO_4^{2-}, and $H_2PO_4^-$. To obtain the concentrations of the five dominant species at $I = 1$ mM as in Fig. 6(b), we first obtain the ratios of the concentrations of the five species to the ionic strength of the mixture as

$$\frac{n_{Na^+}^\infty}{I} = \frac{157}{171.5}, \quad \frac{n_{K^+}^\infty}{I} = \frac{4.5}{171.5},$$
$$\frac{n_{Cl^-}^\infty}{I} = \frac{139.7}{171.5}, \quad \frac{n_{HPO_4^{2-}}^\infty}{I} = \frac{10}{171.5}, \quad \frac{n_{H_2PO_4^-}^\infty}{I} = \frac{1.8}{171.5}. \tag{17}$$

The above ratios remain unchanged for PBS solutions at other ionic strengths. Thus, the concentrations of the five dominant species at $I = 1$ mM can be obtained by multiplying the above ratios to $I = 1$ mM, giving 0.915 mM Na^+, 0.0262 mM K^+, 0.815 mM Cl^-, 0.0583 mM HPO_4^{2-}, and 0.0105 mM $H_2PO_4^-$.

Acknowledgements

References

1 D. C. Prieve, J. L. Anderson, J. P. Ebel and M. E. Lowell, *J. Fluid Mech.*, 1984, **148**, 247–269.

2 D. Velegol, A. Garg, R. Guha, A. Kar and M. Kumar, *Soft Matter*, 2016, **12**, 4686–4703.

3 H. J. Keh, *Curr. Opin. Colloid Interface Sci.*, 2016, **24**, 13–22.

4 E. Lee, *Theory of Electrophoresis and Diffusiophoresis of Highly Charged Colloidal Particles*, Elsevier, New York, 2018.

5 S. Shin, *Phys. Fluids*, 2020, **32**, 101302.

6 S. Shim, *Chem. Rev.*, 2022, **122**, 6986–7009.

7 J. T. Ault and S. Shin, *Annu. Rev. Fluid. Mech.*, 2024, **57**, 227–255.

8 M. Loose, E. Fischer-Friedrich, J. Ries, K. Kruse and P. Schwille, *Science*, 2008, **320**, 789–792.

9 J. Lutkenhaus, *Science*, 2008, **320**, 755–756.

10 R. P. Sear, *Phys. Rev. Lett.*, 2019, **122**, 128101.

11 B. Ramm, A. Goychuk, A. Khmelinskaia, P. Blumhardt, H. Eto, K. A. Ganzinger, E. Frey and P. Schwille, *Nat. Phys.*, 2021, **17**, 850–858.

12 A. Kar, T. Chiang, I. O. Rivera, A. Sen and D. Velegol, *ACS Nano*, 2015, **9**, 746–753.

13 S. W. Park, J. Lee, H. Yoon and S. Shin, *Energy Fuels*, 2021, **35**, 4885–4892.

14 N. Shi and A. Abdel-Fattah, *Phys. Rev. Fluids*, 2021, **6**, 053103.

15 H. Tan, A. Banejee, N. Shi, X. Tang, A. Abdel-Fattah and T. M. Squires, *Sci. Adv.*, 2021, **7**, eabh0638.

16 S. Shin, V. S. Doan and J. Feng, *Phys. Rev. Appl.*, 2019, **12**, 024014.

17 V. S. Doan, S. Chun, J. Feng and S. Shin, *Nano Lett.*, 2021, **21**, 7625–7630.

18 C. Lee, C. Cottin-Bizonne, A. L. Biance, P. Joseph, L. Bocquet and C. Ybert, *Phys. Rev. Lett.*, 2014, **112**, 244501.

19 N. Shi, R. Nery-Azevedo, A. I. Abdel-Fattah and T. M. Squires, *Phys. Rev. Lett.*, 2016, **117**, 258001.

20 S. Shin, E. Um, B. Sabass, J. T. Ault, M. Rahimi, P. B. Warren and H. A. Stone, *Proc. Natl. Acad. Sci. U. S. A.*, 2016, **113**, 257–261.

21 S. Zhai and H. Zhao, *Phys. Rev. E*, 2016, **93**, 052409.

22 S. Shin, J. T. Ault, P. B. Warren and H. A. Stone, *Phys. Rev. X*, 2017, **4**, 041038.

23 F. Raynal, M. Bourgoin, C. Cottin-Bizonne, C. Ybert and R. Volk, *J. Fluid Mech.*, 2018, **847**, 228–243.

24 F. Raynal and R. Volk, *J. Fluid Mech.*, 2019, **876**, 818–829.

25 J. T. Ault, S. Shin and H. A. Stone, *Soft Matter*, 2019, **15**, 1582–1596.

26 A. McMullen, G. Araujo, M. Winter and D. Stein, *Sci. Rep.*, 2019, **9**, 15065.

27 D. Ha, S. Seo, K. Lee and T. Kim, *ACS Nano*, 2019, **13**, 12939–12948.

28 H. C. W. Chu, S. Garoff, R. D. Tilton and A. S. Khair, *Soft Matter*, 2020, **16**, 238–246.

29 M. K. Rasmussen, J. N. Pedersen and R. Marie, *Nat. Commun.*, 2020, **11**, 2337.

30 H. C. W. Chu, S. Garoff, R. D. Tilton and A. S. Khair, *J. Fluid Mech.*, 2021, **917**, A52.

31 N. Singh, G. T. Vladisavljevic, F. Nadal, C. Cottin-Bizonne, C. Pirat and G. Bolognesi, *Phys. Rev. Lett.*, 2020, **125**, 248002.

32 H. C. W. Chu, S. Garoff, R. D. Tilton and A. S. Khair, *Soft Matter*, 2022, **18**, 1896–1910.

33 B. M. Alessio, S. Shim, A. Gupta and H. A. Stone, *J. Fluid Mech.*, 2022, **942**, A23.

34 B. E. McKenzie, H. C. W. Chu, S. Garoff, R. D. Tilton and A. S. Khair, *J. Fluid Mech.*, 2022, **949**, A17.

35 R. Volk, M. Bourgoin, C. Brehier and F. Raynal, *J. Fluid Mech.*, 2022, **948**, A42.

36 J. Xu, Z. Wang and H. C. W. Chu, *RSC Adv.*, 2023, **13**, 9247–9259.

37 B. Akdeniz, J. A. Wood and R. G. H. Lammertink, *Langmuir*, 2023, **39**, 2322–2332.

38 S. Zhang and H. C. W. Chu, *Nanoscale*, 2024, **16**, 9367–9381.

39 J. Teng, B. Rallabandi and J. T. Ault, *J. Fluid Mech.*, 2023, **977**, A5.

40 S. Zhang and H. C. W. Chu, *Chem. Sci.*, 2024, **15**, 18476–18489.

41 H. Liu and A. A. Pahlavan, Solute-mediated colloidal vortex in a microfluidic T-junction, *arXiv*, 2025, preprint, arXiv:2409.01594, DOI: **10.48550/arXiv.2409.01594**.

42 Y. Pawar, Y. E. Solomentsev and J. L. Anderson, *J. Colloid Interface Sci.*, 1993, **155**, 488–498.

43 S. Majhi and S. Bhattacharyya, *Colloids Surf., A*, 2022, **648**, 129272.

44 B. Bhaskar and S. Bhattacharyya, *Phys. Fluids*, 2023, **35**, 062012.

45 J. L. Wilson, S. Shim, Y. E. Yu, A. Gupta and H. A. Stone, *Langmuir*, 2020, **36**, 7014–7020.

46 T. Chiang and D. Velegol, *J. Colloid Interface Sci.*, 2014, **424**, 120–123.

47 A. Gupta, B. Rallabandi and H. A. Stone, *Phys. Rev. Fluids*, 2019, **4**, 043702.

48 H. Ohshima, *Colloid Polym. Sci.*, 2021, **299**, 1877–1884.

49 S. Samanta, P. Mahapatra, H. Ohshima and P. P. Gopmandal, *Phys. Fluids*, 2023, **35**, 032006.

50 S. Sambamoorthy and H. C. W. Chu, *Soft Matter*, 2023, **19**, 1131–1143.

51 B. Bhaskar and S. Bhattacharyya, *Phys. Fluids*, 2023, **35**, 102023.

52 A. Somasundar, B. Qin, S. Shim, B. L. Bassler and H. A. Stone, *ACS Appl. Mater. Interfaces*, 2023, **15**, 33263–33272.

53 M. Jotkar, P. de Anna, M. Dentz and L. Cueto-Felgueroso, *J. Fluid Mech.*, 2024, **991**, A8.

54 M. Jotkar, I. Ben-Noah, J. J. Hidalgo and M. Dentz, *Adv. Water Resour.*, 2024, **193**, 104828.

55 M. Alipour, Y. Li, H. Liu and A. A. Pahlavan, Diffusiophoretic transport of colloids in porous media, *arXiv*, 2025, preprint, arXiv:2411.14712, DOI: **10.48550/arXiv.2411.14712**.

56 H. C. Brinkman, *Appl. Sci. Res.*, 1949, **1**, 27–34.

57 J. Happel and H. Brenner, *Low Reynolds Number Hydrodynamics*, Springer, New York, 1983.

58 R. J. Hunter, *Zeta Potential in Colloid Science*, Academic Press, New York, 1981.

59 S. A. Allison, Y. Xin and H. Pei, *J. Colloid Interface Sci.*, 2007, **313**, 328–337.

60 P. Tsai and E. Lee, *Soft Matter*, 2011, **7**, 5789–5798.

61 J. P. Hsu, C. Huang and S. Tseng, *Chem. Eng. Sci.*, 2012, **84**, 574–579.

62 R. J. Hill, *Soft Matter*, 2016, **12**, 8030–8048.

63 R. W. O'Brien and L. R. White, *J. Chem. Soc. Faraday Trans. II*, 1978, **74**, 1607–1626.

64 R. W. O'Brien and R. J. Hunter, *Can. J. Chem.*, 1981, **81**, 1878–1887.

65 D. C. Prieve and R. Roman, *J. Chem. Soc. Faraday Trans. II*, 1987, **83**, 1287–1306.

66 J. H. Dane and G. C. Topp, *Methods of Soil Analysis Part 4 Physical Methods*, Soil Science Society of America Inc., Madison Wisconsin, 2002.

67 P. G. Righetti and C. Gelfi, *J. Chromatogr. B*, 1996, **699**, 63–75.

68 A. Pluen, P. A. Netti, R. K. Jain and D. A. Berk, *Biophys. J.*, 1999, **77**, 542–552.

69 L. Ramirez, S. R. Gentile, S. Zimmermann and S. Stoll, *J. Colloid Sci. Biotechnol.*, 2016, **5**, 1–9.

70 Y. Chang, Y. Wang and W. Cheng, *Colloid Polym. Sci.*, 2009, **287**, 659–670.

71 A. Kotera, K. Furusawa and Y. Takeda, *Kolloid-Z. Z. Polym.*, 1970, **239**, 677–681.

72 K. Bere, X. Xiong, S. Saringer, G. Douglas and I. Szilagyi, *J. Mol. Liq.*, 2023, **384**, 122285.

73 H. Ono, F. Sato, E. Jidai and K. Shibayama, *Colloid Polym. Sci.*, 1975, **253**, 538–543.

74 W. M. Haynes, *CRC Handbook of Chemistry and Physics*, CRC press, Boca Raton, FL, 2014.